

Accepted Manuscript

Synthesis, photophysical studies, solvatochromic analysis and TDDFT calculations of Diazaspiro compounds

Komal Aggarwal, Jitender M. Khurana

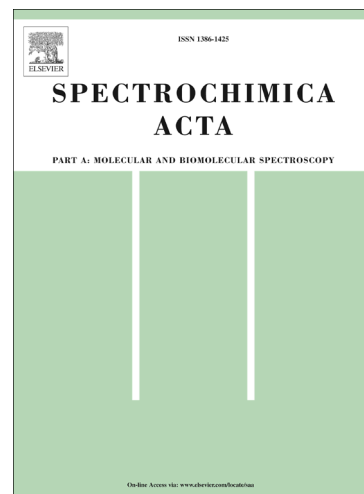
PII: S1386-1425(15)00146-8
DOI: <http://dx.doi.org/10.1016/j.saa.2015.02.004>
Reference: SAA 13293

To appear in: *Spectrochimica Acta Part A: Molecular and Biomolecular Spectroscopy*

Received Date: 6 June 2014
Revised Date: 31 January 2015
Accepted Date: 2 February 2015

Please cite this article as: K. Aggarwal, J.M. Khurana, Synthesis, photophysical studies, solvatochromic analysis and TDDFT calculations of Diazaspiro compounds, *Spectrochimica Acta Part A: Molecular and Biomolecular Spectroscopy* (2015), doi: <http://dx.doi.org/10.1016/j.saa.2015.02.004>

This is a PDF file of an unedited manuscript that has been accepted for publication. As a service to our customers we are providing this early version of the manuscript. The manuscript will undergo copyediting, typesetting, and review of the resulting proof before it is published in its final form. Please note that during the production process errors may be discovered which could affect the content, and all legal disclaimers that apply to the journal pertain.



Synthesis, photophysical studies, solvatochromic analysis and TDDFT calculations of Diazaspiro compounds

Komal Aggarwal and Jitender M. Khurana*

Department of Chemistry, University of Delhi, Delhi-110007, India

*Corresponding author. Tel.: +91 11 2766772; fax: +91 1 27667624

E-mail addresses: jmkhurana1@yahoo.co.in; jmkhurana@chemistry.du.ac.in

Abstract

Diazaspiro[5.5]undecane-1,3,5,9-tetraones and 3-thioxo-diazaspiro[5.5]undecane-1,5,9-trione have been synthesized *via* double Michael addition of 1,5-diphenyl-1,4-pentadien-3-one with active methylene heterocycles *N,N*-dimethyl barbituric acid, barbituric acid and thiobarbituric acid in water:ethanol (1:1) using TBAB as catalyst. The solvent effect on photophysical behavior of these compounds showed that Stokes shift increases with increase in polarity of solvents. The solvent effect on the spectral properties has been investigated by using the Lippert–Mataga and Reichardt methods. The solvatochromism is analyzed by linear solvation energy relationship using the new four-parameter Catalán polarity scales. The relative fluorescence quantum yield of these diazaspiro compounds varies in solvents of different polarity. The HOMO and LUMO energies have been calculated by TDDFT (B3LYP/6-311G(d, p)) approach. TDDFT calculations were also used to compare the experimental and theoretical absorption spectra.

Keywords

Diazaspiro compounds, Catalán polarity scale, dipole moment, HOMO-LUMO, TDDFT

1. Introduction

The effect of solvent on the absorption and fluorescence properties of organic compounds has been a subject of several investigations [1-5]. These investigations have considerable importance in the field of photophysical studies and photochemistry. The effect of solvents on absorption and fluorescence spectra can be used to determine the electric dipole moment of solute molecules which is a direct measure of the electron distribution in a molecule. The excited state dipole moment of a molecule reveals information on the electronic and geometrical structures of the molecule in the short-lived excited state. Knowledge of dipole moments of first electronically excited singlet state of the molecules is quite useful in designing materials with nonlinear optical properties [6], and elucidating the nature of the

excited states. It also indicates the charge distribution in the molecule and is also useful for predicting the site of attack by electrophilic and nucleophilic reagents in some photochemical reactions.

Solvatochromism is an experimentally simple and widely accepted method [7-12], as it does not use any external field [13-14]. This method [15-18], based on the shift of the absorption and fluorescence maxima in various media, provides a reliable way to estimate ground and excited state dipole moment compared to conventional methods like electric dichroism [19], fluorescence polarisation [20], stark splitting of rotational levels [21], microwave conductivity [22], and thermochromic shift method [23].

Extensive photophysical investigation of newly synthesized fluorophores is an essential tool to extract the necessary information about the molecules. Heterocyclic spiro compounds containing nitrogen have interesting conformational features and also show pharmaceutical properties [24-25]. Barbiturates have shown a wide array of CNS drugs such as sedative, anticonvulsant, anxiolytic, anesthetic, antiepileptic [26-28]. They have also been used as a disperse dye with strong fluorescence, as yellow organic pigment [29] and investigated as stain developers for the identification of nucleic acids [30-31]. Similarly, diazasp[5.5]undecane-1,3,5,9-tetraones and 3-thioxo-2,4 diazasp[5.5]undecane-1,5,9-triones show wide range of biological and therapeutic properties such as antibacterial [32], fungicidal [33], potent sedative-hypnotic [34], CNS depressants [35] and anticonvulsant [36]. The various biological applications of barbiturates and diazasp[5.5]undecane compounds encouraged us to investigate the solvatochromic behaviour of these molecules.

Literature survey revealed that there are no reports available on the photophysical studies and determination of μ_g and μ_e values of the investigated molecules. In this paper, we report a simple and efficient synthesis of diazasp[5.5]undecane compounds containing barbiturates/thiobarbiturates *via* the double Michael addition of dibenzalacetone derivatives with *N,N*-dimethylbarbituric acid/barbituric acid/thiobarbituric acid in ethanol: water (1:1) using 10 mol% of TBAB under reflux. Solvatochromic behaviour of three diazasp[5.5]undecane compounds with different substituents on barbituric acid moiety was studied. The results were used to obtain the ground and excited state dipole moments. The solvent effects were analyzed using Lippert-Mataga, Reichardt equation and also with the new four-parameter Catalán polarity scales. We have also carried out the TDDFT (time-dependent density functional theory) calculations of spiro derivatives to calculate the electronic excitation energies and a comparative study of the experimental absorption spectra with TDDFT calculations.

2. Experimental

All the starting materials were of GR (Guaranteed Reagent) quality of Merck and all solvents used were HPLC grade. Melting points were determined on a Tropical Lab equip apparatus and are uncorrected. The ^1H NMR spectrum was recorded on Jeol JNM ECX-400P at 400 MHz using TMS as an internal standard. The chemical shift values are recorded on δ scale and the coupling constants (J) are in Hertz. Solvents were checked in steady-state fluorescence apparatus for any fluorescence impurities in the wavelength ranges of interest. UV-vis absorption spectra were recorded on an Analytikjena Specord 250 spectrophotometer. Fluorescence spectra were measured at Cary Eclipse fluorescence spectrophotometer. All spectroscopic measurements were done at room temperature. HPLC purification was done on Shimadzu analytical HPLC system of synthesized diazaspino compounds using 90:10 (water: acetonitrile) solvent system with flow rate 1 mL/min. The photophysical properties of the diazaspino compounds (**3a-c**) were recorded in dilute concentrations (5×10^{-5} M).

2.1. General procedure for the synthesis of diazaspino compounds

In a general procedure, dibenzylidene acetone (1 mmol), *N,N*-dimethyl barbituric acid/ barbituric acid/ thiobarbituric acid (1 mmol) and 4 mL of ethanol: water (1:1) were taken in a 50 mL round-bottomed flask. 10 mol% of Tetrabutyl ammonium bromide (TBAB) was added to the mixture, and the contents were stirred. The reaction mixture was refluxed and the progress of the reaction was monitored by TLC using ethyl acetate: petroleum ether (30: 70) as eluent for disappearance of active methylene compounds. After completion of the reaction, the reaction mixture was allowed to cool to room temperature and diluted with water (5 mL). The solid obtained was filtered at pump and washed with water: ethanol (2:1). The product was recrystallized with ethanol. The products were characterized by their spectral data.

2.2. Spectral data

2.2.1. 7,11-Diphenyl-2,4-diazaspino[5.5]undecane-1,3,5,9-tetraone (**3a**)[37(a)]

White solid, Yield: 86%, M.p. 275-277°C (Lit. M.p. 272-273°C); ^1H NMR (400 MHz, DMSO- d_6) : 2.44, 2.48 (dd, 2H, $J = 15.4$ Hz, 4.4 Hz), 3.49 (t, 2H, $J = 14.6$ Hz), 3.96, 3.99 (dd, 2H, $J = 14.3$ Hz, 4.4 Hz), 7.13 (d, 4H, Ar-H, $J = 7.3$ Hz), 7.27 - 7.34 (m, 6H, Ar-H), 11.20 (s, 1H, -NH), 11.46 (s, 1H, -NH).

2.2.2. 2,4-Dimethyl-7,11-diphenyl-2,4-diazaspino[5.5]undecane-1,3,5,9-tetraone (**3b**) [33]

White solid, Yield: 89%, M.p. 150-152°C (Lit. M.p. 150-152°C); ¹H NMR (400 MHz, CDCl₃) δ : 2.59, 2.63 (dd, 2H, *J* = 14.6 Hz, 4.4 Hz), 2.86 (s, 3H, -NCH₃), 3.01 (s, 3H, -NCH₃), 3.69 (t, 2H, *J* = 14.6 Hz), 3.99, 4.03 (dd, 2H, *J* = 13.9 Hz, 4.4 Hz), 7.05-7.07 (m, 4H, Ar-H), 7.23-7.26 (m, 6H, Ar-H).

2.2.3. 7,11-Diphenyl-3-thioxo-2,4-diazaspiro[5.5]undecane-1,5,9-trione (3c) [37(b)]

White solid, Yield: 84%, M.p. 254-256°C (Lit. M.p. 250-252°C); ¹H NMR (400 MHz, CDCl₃) δ : 2.62, 2.66 (dd, 2H, *J* = 15.4 Hz, 4.4 Hz), 3.64 (t, 2H, *J* = 15.4 Hz), 3.95, 3.99 (dd, 2H, *J* = 14.7 Hz, 4.4 Hz), 7.12-7.15 (m, 4H, Ar-H), 7.27 - 7.28 (m, 6H, Ar-H), 8.35 (s, 1H, -NH), 8.55 (s, 1H, -NH).

2.3. Computational details

The hybrid density functional B3LYP (Becke–Lee–Young–Parr composite of exchange-correction functional) method [38] and the standard 6–311G (d, p) basis set were used for structure optimization. All the theoretical calculations are performed with GAUSSIAN 09W software package [39]. The theoretical electronic properties (HOMO–LUMO energies, absorption wavelengths) were performed using the TDDFT [40-42] in vacuum using the same B3LYP level and basis set.

2.4. Methods

Experimental calculations of ground state and excited state dipole moments

We have employed the fluorescence solvatochromic shift method [15-18] to measure the stabilization of the excited states of **3a-c**. The change of magnitudes for dipole moments between ground and excited states, i.e., $\Delta\mu = \mu_e - \mu_g$, can be estimated by the Lippert-Mataga equation (1) and expressed as [43-44]:

$$\bar{\nu}_a - \bar{\nu}_f = \frac{2(\mu_e - \mu_g)^2}{hca^3} (\Delta f) + \text{constant} \quad (1)$$

where, $\bar{\nu}_a$ and $\bar{\nu}_f$ are the wavenumbers of the absorption and emission maxima respectively.

$$\Delta f = f(\epsilon) - f(n^2) = \frac{\epsilon - 1}{2\epsilon + 1} - \frac{n^2 - 1}{2n^2 + 1} \quad (2)$$

When specific fluorophore/solvent interactions such as hydrogen bonding or electron-pair donor/electron-pair acceptor interactions also contribute significantly in addition to the non-specific interactions, then the Lippert-Mataga equation is no longer applicable. In that case, the dipole moment change between the excited and ground state can be estimated by

correlating the Stokes shift with the microscopic solvent polarity parameter E_T^N as proposed by Reichardt [45] and developed by Ravi *et al.* [46].

In empirical molecular-microscopic solvent polarity parameter (E_T^N), the problem associated with the Onsager's radius estimation can be minimized since a ratio of two Onsager's radii is involved according to eq. (3):

$$\Delta\bar{\nu} = \bar{\nu}_a - \bar{\nu}_f = 11307.6 \left[\left(\frac{\Delta\mu}{\Delta\mu_B} \right)^2 \left(\frac{a_B}{a} \right)^3 \right] E_T^N + \text{constant} \quad (3)$$

where $\Delta\mu_B$ (9 D) and a_B (6.2 Å) are the dipole moment change ($\Delta\mu = \mu_e - \mu_g$) and Onsager's radius, respectively, for a pyridinium *N*-phenolate betaine dye used to determine the E_T^N values, whereas $\Delta\mu$ and a are the corresponding quantities for the molecule under study. The change in dipole moment $\Delta\mu$ can be evaluated from the slope of the Stokes shift versus E_T^N plot and is given by eq. (4):

$$\Delta\mu = (\mu_e - \mu_g) = \sqrt{\frac{m \times 81}{11307.6 (6.2/a)^3}} \quad (4)$$

where 'm' is the slope obtained from the plot of Stokes shift versus microscopic solvent polarity (E_T^N) using eq. (3).

The following equations have been used to determine the excited state (μ_e) and ground state (μ_g) dipole moments by solvatochromic method. These equations have been obtained by employing the quantum-mechanical second order perturbation theory of a spherical solute and also considering the Onsager's model of reaction field for a polarizable dipole moment.

Bakhshiev's equation [10]

$$\bar{\nu}_a - \bar{\nu}_f = m_1 F_1(\epsilon, n) + \text{constant} \quad (5)$$

Kawski-Chamma-Viallet equation [11-12]

$$\frac{\bar{\nu}_a + \bar{\nu}_f}{2} = -m_2 F_2(\epsilon, n) + \text{constant} \quad (6)$$

where, $\bar{\nu}_a$ and $\bar{\nu}_f$ are wavenumbers of the absorption and emission maxima, respectively, and

$$F_1(\epsilon, n) = \frac{n^2 + 1}{n^2 + 2} \left[\frac{\epsilon - 1}{\epsilon + 2} - \frac{n^2 - 1}{n^2 + 2} \right] \quad (7)$$

$$F_2(\epsilon, n) = \frac{2n^2 + 1}{2(n^2 + 2)} \left[\frac{\epsilon - 1}{\epsilon + 2} - \frac{n^2 - 1}{n^2 + 2} \right] + \frac{3}{2} \left[\frac{n^4 - 1}{(n^2 + 2)^2} \right] \quad (8)$$

where, $F_1(\varepsilon, n)$ and $F_2(\varepsilon, n)$ are Bakhshiev polarity function and Kawski-Chamma-Viallet polarity function, respectively.

$$m_1 = \frac{2(\mu_e - \mu_g)^2}{hca_0^3} \quad (9)$$

$$m_2 = \frac{2(\mu_e^2 - \mu_g^2)}{hca_0^3} \quad (10)$$

where, m_1 and m_2 are the slopes which can be calculated from equations (5) and (6), respectively, h is Planck's constant, c is the speed of light in vacuum, a_0 is the radius of the cavity in which the fluorophore resides, and μ_e and μ_g are the dipole moments in the excited and ground states, respectively, ε and n are the dielectric constant and the index of refraction of the solvents, respectively. Onsager cavity radii (a_0) for investigated molecules were determined theoretically according to their optimized geometry using DFT at B3LYP/6-311G (d, p) basis set.

If the ground state and excited state dipole moments are parallel, the following expressions are obtained on the basis of (9) and (10):

$$\mu_g = \frac{|m_2 - m_1|}{2} \left(\frac{hca_0^3}{2m_1} \right)^{1/2} \quad (11)$$

$$\mu_e = \frac{|m_2 + m_1|}{2} \left(\frac{hca_0^3}{2m_1} \right)^{1/2} \quad (12)$$

Therefore, the ratio of excited state dipole moment to the ground state dipole moment can be expressed as (eq. 13):

$$\frac{\mu_e}{\mu_g} = \left| \frac{m_2 + m_1}{m_2 - m_1} \right| \quad (13)$$

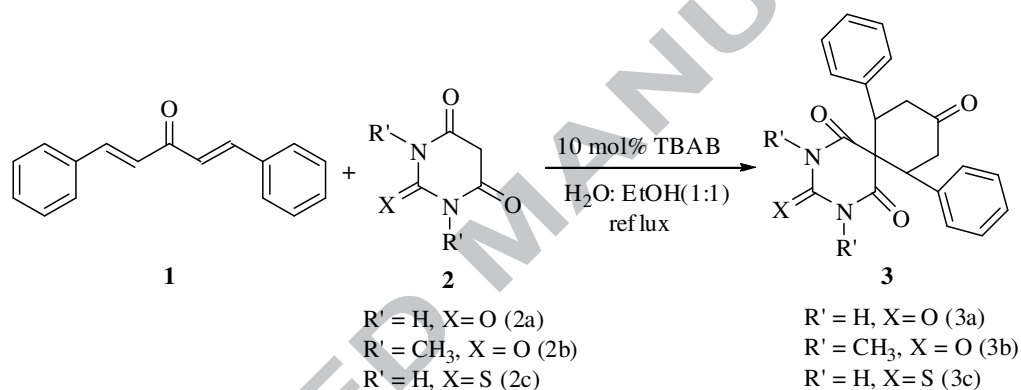
For the determination of the relative fluorescence quantum yield (Φ_f) of **3a**, **3b** and **3c** in solvents having different polarity and hydrogen bonding ability, only dilute solutions with an absorbance below 0.1 at the excitation wavelength ($\lambda_{ex} = 270$ nm for **3a**, $\lambda_{ex} = 272$ nm for **3b** and $\lambda_{ex} = 280$ nm for **3c**) were used. For the Φ_f determinations of all the three compounds, 2-amino pyridine in 1N sulphuric acid ($\Phi_f = 0.60$) was used as fluorescence standard and calculated on the basis of the equation (14) [46], where n_0 and n are the refractive indices of the solvents, A^0 and A are the absorbances, Φ_f^0 and Φ_f are the fluorescence quantum yields and

the integrals denote the area of the fluorescence band for the standard and the sample, respectively.

$$\Phi_f = \Phi_f^0 \frac{n^2 A^0 \int I_f(\lambda_f) d\lambda_f}{n_0^2 A \int I_f^0(\lambda_f) d\lambda_f} \quad (14)$$

3. Results and discussion

Nitrogen containing spiro heterocycles having barbituric acid, *N,N*-dimethyl barbituric acid and thiobarbituric acid moiety were particularly chosen in this study. The diazaspino compounds were synthesized as outlined in Scheme 1. The molecular structures of all three diazaspino compounds (**3a-c**) as identified by spectral data and the optimized molecular geometries calculated by quantum chemical calculations at DFT/B3LYP (6-311G (d,p)) are shown in Fig. 1 and Fig. 2, respectively.



Scheme 1: Double Michael addition of dibenzylidene acetone with barbituric acid, *N,N*-dimethyl and thiobarbituric acid.

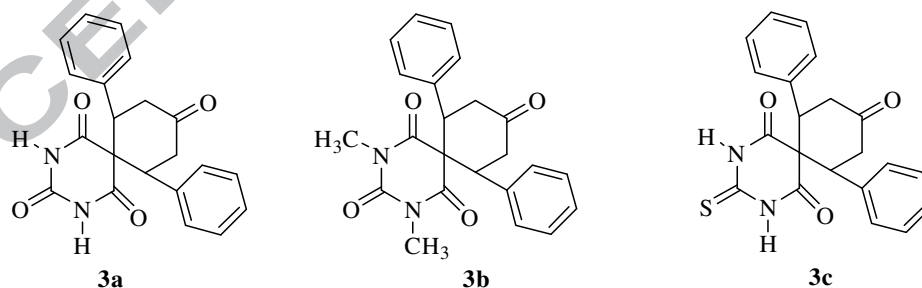


Fig. 1: Structures of compounds **3a**, **3b** and **3c**.

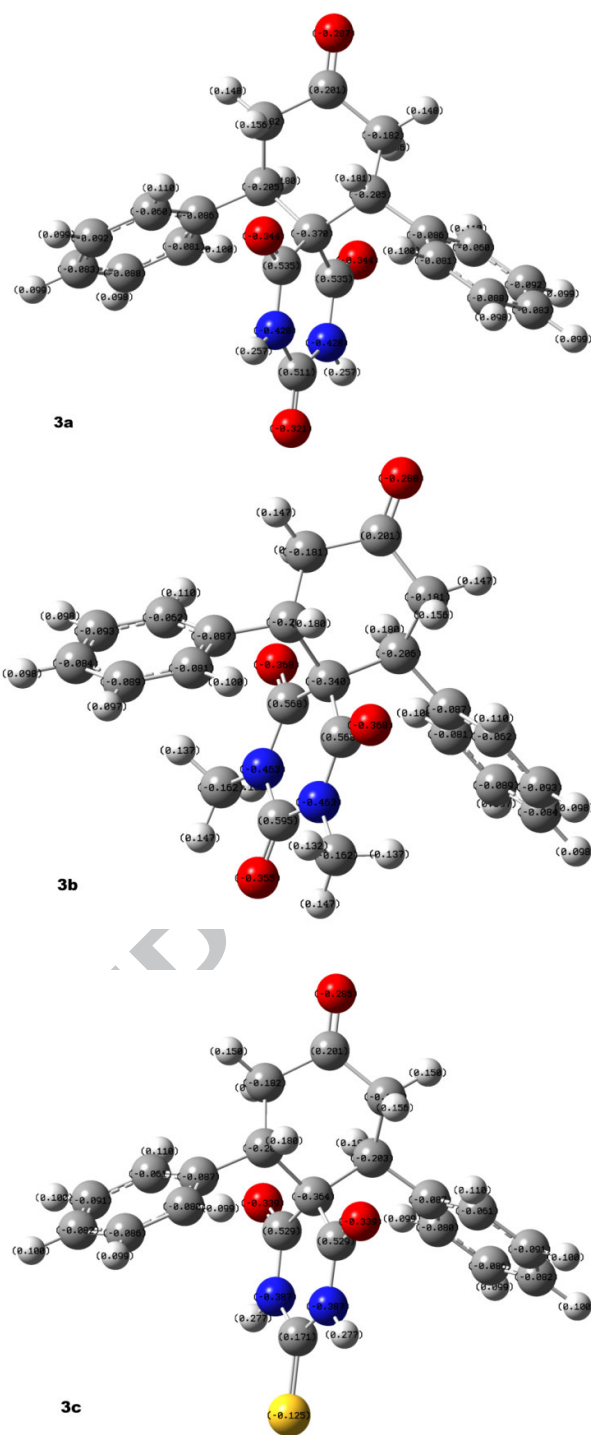


Fig. 2: Optimized geometries for the lowest-lying state (S_0) of **3a**, **3b** and **3c** at the B3LYP/6-311G (d,p) level.

UV-visible absorption maxima ($\lambda_{\text{abs}}/\text{nm}$), fluorescence emission maxima ($\lambda_{\text{em}}/\text{nm}$), Stokes shift ($\bar{\nu}_a - \bar{\nu}_f/\text{cm}^{-1}$) and quantum yield (Φ_f) of **3a**, **3b** and **3c** in a series of solvents of varying polarity are given in Table 1.

Table 1: UV-vis spectroscopic and photophysical properties of **3a**, **3b** and **3c** in different solvents

Comp. No.	Solvents	$\bar{\nu}_a/\text{cm}^{-1}$ ($\lambda_{\text{abs}}/\text{nm}$)	$\bar{\nu}_f/\text{cm}^{-1}$ ($\lambda_{\text{em}}/\text{nm}$)	$\bar{\nu}_a - \bar{\nu}_f/\text{cm}^{-1}$	$(\bar{\nu}_a + \bar{\nu}_f)/2 \text{ cm}^{-1}$	Φ_f
3a	MeOH	36765 (272)	24096 (415)	12669	30430	0.076
	ACN	36765 (272)	24213 (413)	12552	30489	0.082
	DMF	36900 (271)	24449 (409)	12451	30674	0.086
	DCM	36900 (271)	24630 (406)	12330	30765	0.095
	CHCl ₃	37037 (270)	24752 (404)	12285	30894	0.077
	DIOX	37175 (269)	25188 (397)	11987	31181	0.069
	n-HEPT	37175 (269)	25316 (395)	11859	31245	0.065
3b	MeOH	36232 (276)	24038 (416)	12192	30134	0.067
	ACN	36363 (275)	24271 (412)	12092	30317	0.050
	DMF	36232 (276)	24154 (414)	12077	30192	0.056
	DCM	36496 (274)	24449 (409)	12047	30472	0.074
	CHCl ₃	36765 (272)	24752 (404)	12012	30758	0.062
	DIOX	36765 (272)	24813 (403)	11951	30788	0.052
	n-HEPT	37037 (270)	25125 (398)	11919	31081	0.045
3c	MeOH	35971 (278)	23752 (421)	12219	29861	0.081
	ACN	35587 (281)	23980 (417)	11607	29780	0.062
	DMF	35587 (281)	24154 (414)	11433	29870	0.073
	DCM	35461 (282)	24213 (413)	11248	29837	0.078
	CHCl ₃	35461 (282)	24509 (408)	10952	29985	0.058
	DIOX	35461 (282)	24630 (406)	10831	30045	0.046
	n-HEPT	35714 (280)	25380 (394)	10333	30547	0.042

3.1. Solvent effect on the absorption and fluorescence spectra

The solvatochromic properties of **3a**, **3b** and **3c**, their UV-vis and fluorescence spectra were measured in solvents of different polarity. Typical absorption and fluorescence spectra of **3a**, **3b** and **3c** in different solvents are shown in Figs. 3, 4 and 5, respectively. All the three diazaspino compounds (**3a-c**) showed a broad absorption band in 250–300 nm spectral range with a peak position centered at 270 nm. The absorption band showed moderate sensitivity (4-10 nm) towards both solvent polarity and the substituents. Thus it can be concluded that the substitution and solvent effects are negligible in the ground state of the molecules.

On increasing solvent polarity from *n*-heptane to methanol, the emission peak maxima of **3a**, **3b** and **3c** are more readily shifted towards longer wavelengths i.e. for **3a** it red shifted from 395 to 415 nm, for **3b** from 398 to 416 nm and for **3c** from 394 to 421 nm corresponding to 20, 18 and 23 nm bathochromic shift of the emission maximum of the **3a**, **3b** and **3c**, respectively, confirming a π - π^* transition. The shift of the emission maxima towards longer wavelengths could be due to the marked difference between the excited state and ground state charge distribution in the solute, resulting in stronger interaction with polar solvents in the excited state and also to a higher dipole moment in the excited state.

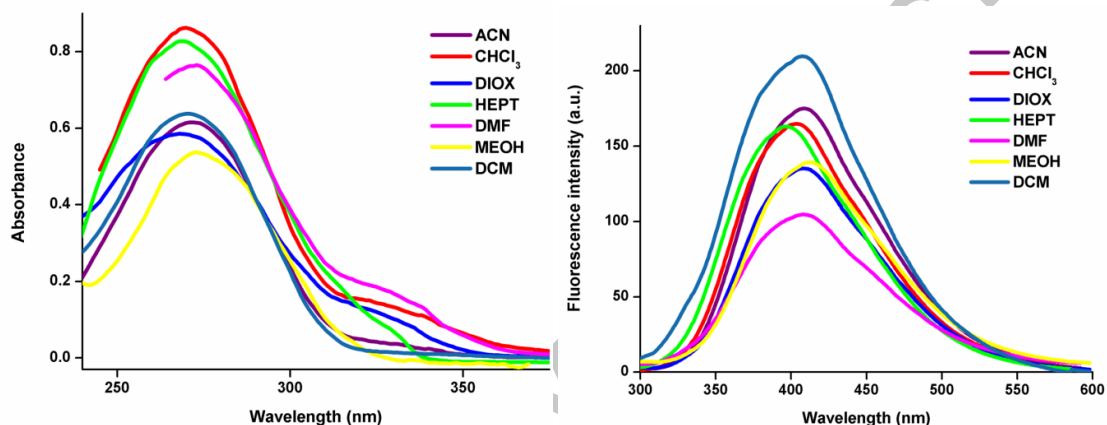


Fig. 3: Absorption and fluorescence spectra of compound **3a** in MeOH, ACN, DMF, DCM, CHCl_3 , DIOX and *n*-HEPT. Excitation wavelength: 270 nm.

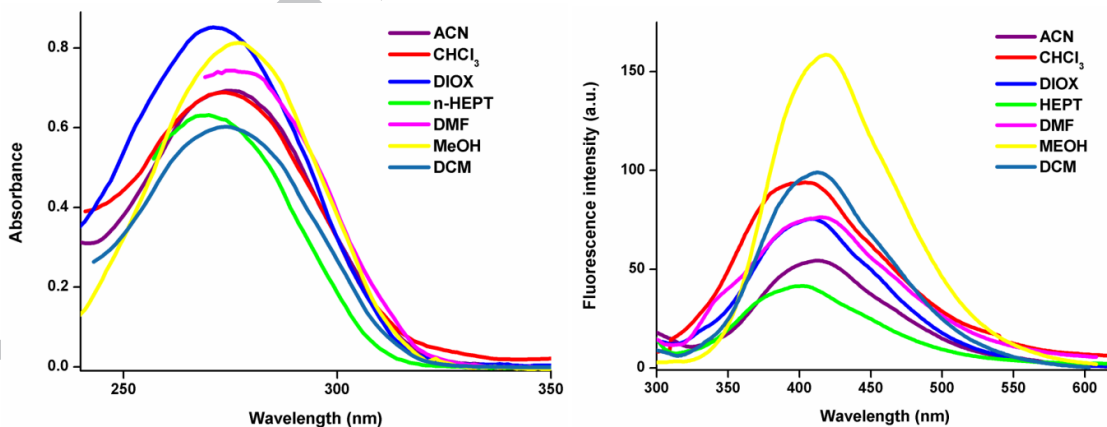


Fig. 4: Absorption and fluorescence spectra of compound **3b** in MeOH, ACN, DMF, DCM, CHCl_3 , DIOX and *n*-HEPT. Excitation wavelength: 272 nm.

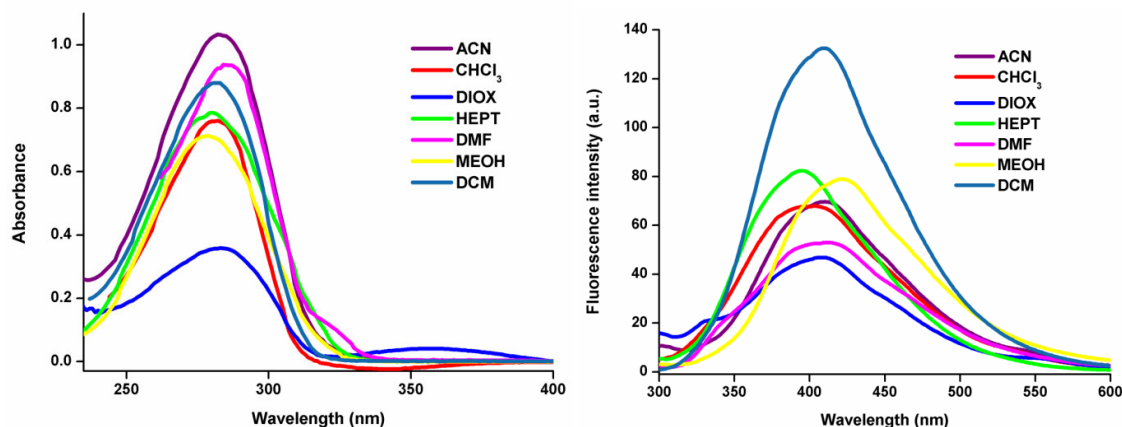


Fig. 5: Absorption and fluorescence spectra of compound **3c** in MeOH, ACN, DMF, DCM, CHCl_3 , DIOX and *n*-HEPT. Excitation wavelength: 280 nm.

It can be observed from Table 1 that increasing solvent polarity from *n*-heptane to methanol resulted in an increase of Stokes shift by 810, 273 and 1886 cm^{-1} for **3a**, **3b** and **3c**, respectively, which is indicative of charge transfer transition and increase in the dipole moment on excitation. The large magnitude of Stokes shift also indicates that the excited state geometry could be different from ground state. It can be inferred from Table 1 that the higher Stokes shift observed in polar protic methanol compared to polar aprotic acetonitrile, indicates that hydrogen bonding interactions predominate over dipolar interactions.

3.2. Correlation of Solvatochromic shift with solvent polarity parameters

The plot of the Stokes shift ($\bar{\nu}_a - \bar{\nu}_f$) as a function of Δf is sufficiently linear with excellent correlation for **3a-c** (Fig. 6(a)). Accordingly, $\Delta\mu = \mu_e - \mu_g$ values have been calculated as 5.97 D, 3.81 D and 7.93 D for **3a**, **3b** and **3c**, respectively. The linear correlation of Stokes shifts vs E_T^N plotted for the solvents used in this study (Fig. 6(b)), is a clear evidence of the existence of general solute-solvent interactions and H-bonding interactions in the polar solvents.

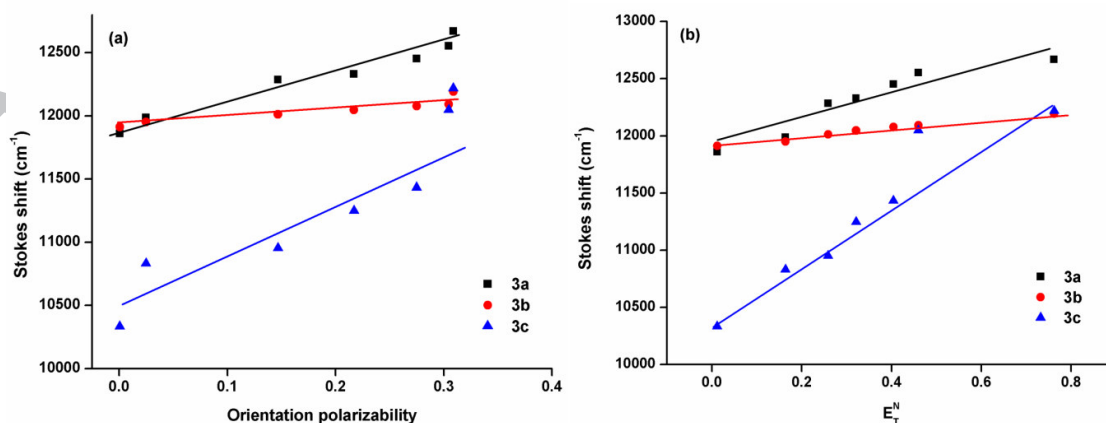


Fig. 6 (a) Plot of Stokes shift vs. Orientation polarizability (Δf) of 3a, 3b and 3c. (b) Plot of Stokes shift vs. Reichardt's solvent polarity function E_T^N of 3a, 3b and 3c.

The slopes obtained by plotting Stokes shift vs. orientation polarizability (Δf) (Lippert-Mataga Correlation) (Fig. 6a)/ molecular-microscopic solvent polarity parameter (E_T^N) (Reichardt Correlation) (Fig. 6b)/ solvent polarity function $F_1(\epsilon, n)$ (Bakhshiev Correlation) (Fig. 7a) and spectral shift $(\bar{\nu}_a + \bar{\nu}_f)/2$ vs. solvent polarity function $F_2(\epsilon, n)$ (Kawski-Chamma-Viallet Correlation) (Fig. 7b), of compounds **3a**, **3b** and **3c** are given in Table 2.

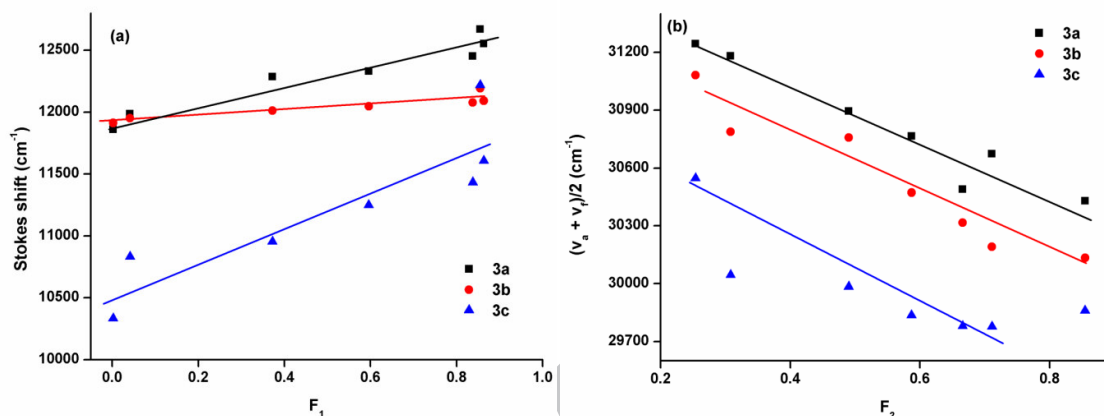


Fig. 7: (a) Variation of Stokes shift with $F_1(\epsilon, n)$ by using Bakhshiev's equation in different solvents for 3a, 3b and 3c. (b) The variation of arithmetic mean of $\bar{\nu}_a$ and $\bar{\nu}_f$ with $F_2(\epsilon, n)$ by using Kawski-Chamma-Viallet's equation in different solvents for 3a, 3b and 3c.

Table 2: Slopes obtained by Lippert-Mataga, Reichardt, Bakhshiev and Kawski-Chamma-Viallet (K-C-V) Correlations

	Comp.	Slope (cm ⁻¹)	Intercept (cm ⁻¹)	Correlation coefficient (<i>r</i>)	No. of data
Lippert-Mataga Correlation	3a	2229.25	11897.62	0.98	7
	3b	676.69	11916.86	0.93	7
	3c	3460.10	10508.35	0.95	6
Reichardt Correlation	3a	1157.66	11910.78	0.94	7
	3b	387.45	11908.58	0.99	7
	3c	2520.60	10374.13	0.99	7
Bakhshiev Correlation	3a	749.96	11922.50	0.96	7
	3b	227.06	11924.71	0.91	7
	3c	1153.35	10545.84	0.94	6
K-C-V Correlation	3a	1412.55	31592.10	0.97	7
	3b	1557.53	31395.68	0.96	7
	3c	1250.32	30639.05	0.84	6

From the slope m (eq. 4, Table 2), the difference between dipole moments ($\Delta\mu = \mu_e - \mu_g$) are 2.36, 1.58 and 3.75 D for **3a**, **3b** and **3c**, respectively (Table 3). The linear behavior of Stokes shift versus solvent polarity functions (F_1 and F_2) indicates general solvent effects as a function of the dielectric constant and refractive index. The slopes (m_1 and m_2) were taken into account for calculating the ground and excited states dipole moments (μ_g and μ_e) of all the three compounds (**3a-c**).

The μ_g and μ_e values obtained from (eq. 11) and (eq. 12) and the ratio of μ_e and μ_g obtained from (eq. 13) are presented in Table 3. The change in dipole moment values, $\Delta\mu$, estimated using the Lippert-Mataga, Reichardt's, Bakhshiev's and Kawski-Chamma-Viallet correlations are also given in Table 3. The ground state dipole moments of **3a-c** were also computationally optimized by quantum chemical calculations using Gaussian 09 program [39] at DFT/B3LYP (6-311G (d, p)) and the corresponding optimized molecular geometries are shown in Fig. 2.

Table 3: Onsager cavity radius (a_o), ground state (μ_g), excited state (μ_e), dipole moment change ($\Delta\mu$) and dipole moment ratio (μ_e/μ_g) of compounds **3a**, **3b** and **3c**.

	a_o (Å)	μ_g^a	μ_g^b	μ_e^c	$\Delta\mu^d$	$\Delta\mu^e$	$\Delta\mu^f$	$\Delta\mu^g$	$(\mu_e/\mu_g)^h$
3a	5.44	2.77	1.53	4.99	5.97	2.36	3.46	4.75	3.26
3b	6.00	3.59	6.46	8.67	3.81	1.58	2.21	5.78	1.34
3c	5.68	1.97	0.39	4.77	7.93	3.73	4.58	4.77	12.23

Note: 1 Debye (D) = $3.335\ 64 \times 10^{-30}$ C.m

^aCalculated by Gaussian09 software.

^bThe experimental ground states dipole moment calculated from equation (11).

^cThe experimental excited state dipole moment calculated from equation (12).

^dThe change in dipole moment calculated from Lippert's equation (1).

^eThe change in dipole moment calculated from Reichardt's equation (4).

^fThe change in dipole moment calculated from Bakhshiev's equation (9).

^gThe change in dipole moment calculated from Chamma-Viallet's equation (10).

^hThe ratio of excited state and ground state dipole moments values calculated using (13).

It is observed from Table 3 that, $\Delta\mu$ values are highest by Lippert–Mataga method compared to all other methods. This is due to the fact that, this method does not consider polarizability of the solute. The charge separation in a compound **3b** led to the highest excited state dipole moment (Table 3). In case of compounds **3a** and **3c** only tautomeric structures are possible (Fig. 8) resulting in a lower excited state dipole moment compared to **3b**. All the results show a significant increase in the dipole moment on excitation. Thus, a relatively large charge transfer takes place during the excitation of the diazaspiron compounds.

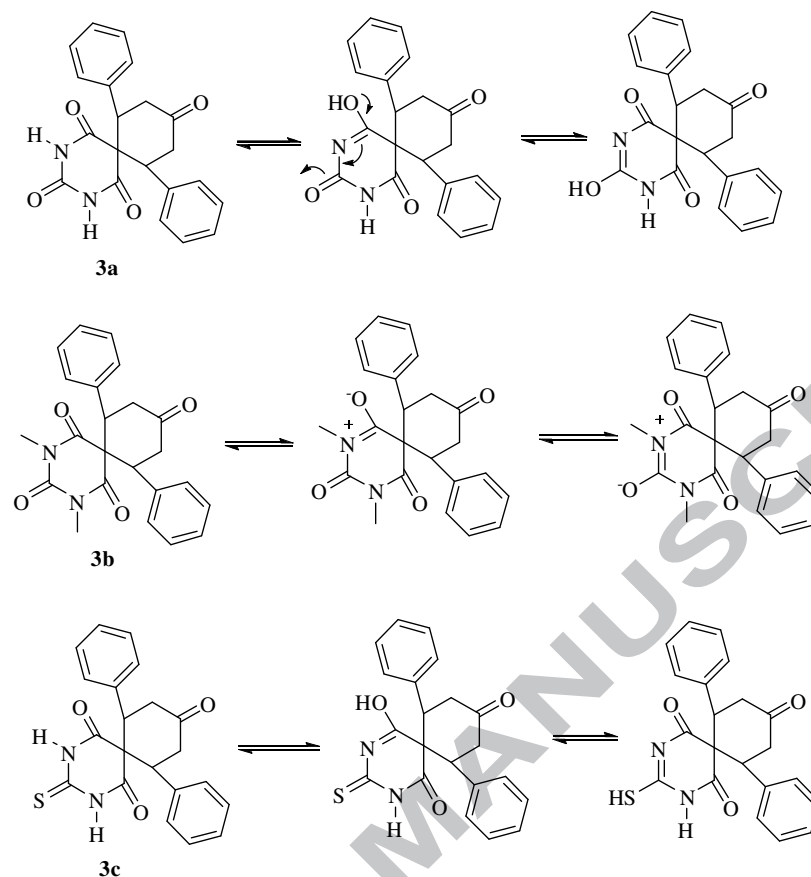


Fig. 8: Possible resonating or tautomeric structures of **3a**, **3b** and **3c**.

The multi parametric approach of Kamlet and Taft has been used [48] to determine the contribution of various modes of solvation (i.e. specific and nonspecific) towards the Stokes shift values. This method involves the effect of individual solvent parameters (hydrogen bond donor, hydrogen bond acceptor and dielectric effects) on the spectral properties of the compounds. The Kamlet–Abboud–Taft relationship is given by eq. 15:

$$\Delta\nu = \Delta\nu_0 + a\alpha + b\beta + c\pi^* \quad (15)$$

where α is an index of hydrogen bond donating ability of the solvent, β is an index of hydrogen bond accepting capacity of the solvent and π^* is the polarity/polarizability parameter of the solvents. The coefficients a , b and c are measure of the sensitivity to each individual contributing parameter. The disadvantage of the Kamlet-Abboud-Taft approach is that the dipolarity and polarizability of the solvent are included in only one parameter (π^*). Recently, Catalán [49] proposed another multiparameter equation, which comprises two parameters for specific and two parameters for non-specific interactions including separate consideration of solvent polarizability (SP) and dipolarity (SdP) (eq. 16).

$$y = y_0 + a.SA + b.SB + c.SP + d.SdP \quad (16)$$

where y denoted a solvent-dependent physicochemical property in a given solvent and y_0 the statistical quantity corresponding to the value of property in the gas phase, SA and SB correspond to the Kamlet–Taft parameter α and β .

Multivariate regression for **3a**, **3b** and **3c** were calculated to fit the values of absorbance maxima, emission maxima and the Stokes shift to the Catalán relationships, the estimated Catalán coefficients (a_{SA} , b_{SB} , c_{SP} , d_{SdP}) and correlation coefficients (r) are listed in Table 4.

Table 4: Adjusted coefficients (y_0 , a_{SA} , b_{SB} , c_{SP} , d_{SdP}) and correlation coefficients (r) for the multiple linear regression analysis of the $\bar{\nu}_a$, $\bar{\nu}_f$ and Stokes shift ($\bar{\nu}_a - \bar{\nu}_f$) of **3a**, **3b** and **3c** as a function of Catalán four-parameter solvent scales.

	y	y_0	a_{SA}	b_{SB}	c_{SP}	d_{SdP}	r
3a	$\bar{\nu}_a$	36629.6 ± 163.0	-52.3 ± 85.9	145.3 ± 72.1	846.9 ± 234.2	-471.8 ± 43.6	0.99
	$\bar{\nu}_f$	24419.8 ± 165.4	-389.3 ± 87.1	250.7 ± 73.2	1381.4 ± 237.6	-1178.3 ± 44.2	0.99
	$\Delta\bar{\nu}$	12145.5 ± 154.6	355.1 ± 81.5	-162.2 ± 68.4	-432.1 ± 222.2	730.2 ± 41.3	0.99
3b	$\bar{\nu}_a$	36837.9 ± 332.1	-47.3 ± 175.0	-416.5 ± 147.0	398.4 ± 477.2	-645.5 ± 88.8	0.99
	$\bar{\nu}_f$	24857.8 ± 349.7	-244.9 ± 184.3	-409.5 ± 154.8	506.8 ± 502.5	-835.9 ± 93.5	0.99
	$\Delta\bar{\nu}$	12002.1 ± 27.7	191.2 ± 14.6	-10.1 ± 12.2	-133.7 ± 39.8	178.0 ± 7.4	0.99
3c	$\bar{\nu}_a$	36471.8 ± 489.0	467.9 ± 257.7	103.9 ± 216.4	-1296.1 ± 707.6	-57.7 ± 130.8	0.91
	$\bar{\nu}_f$	25499.1 ± 1081.2	-661.0 ± 569.8	-141.7 ± 478.5	-358.3 ± 1553.6	-1162.3 ± 289.3	0.95
	$\Delta\bar{\nu}$	10970.0 ± 601.2	1129.3 ± 316.8	245.8 ± 266.1	-934.9 ± 863.8	1105.2 ± 160.8	0.99

The linear correlation between the experimental absorbance, fluorescence and Stokes shift with the corresponding calculated values using all the parameters of Catalán four parameter solvent scale are shown in Figs. 9, 10 and 11, respectively.

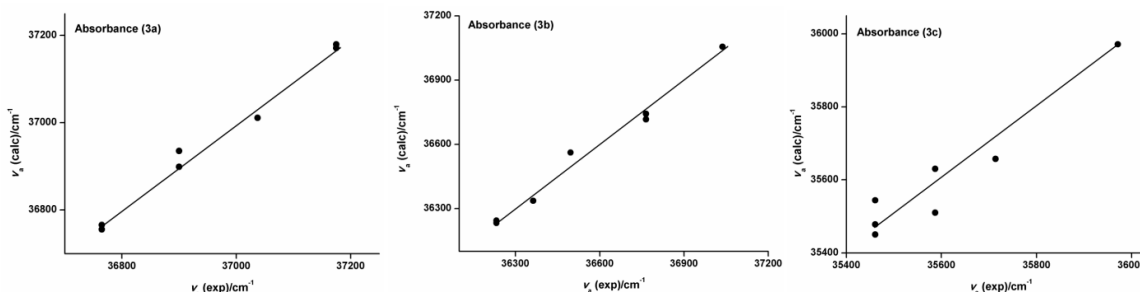


Fig. 9: Correlation between the experimental absorption values with the calculated values obtained by a multicomponent linear regression using the SA, SB, SP and SdP – scale (Catalán) solvent parameters for **3a**, **3b** and **3c**.

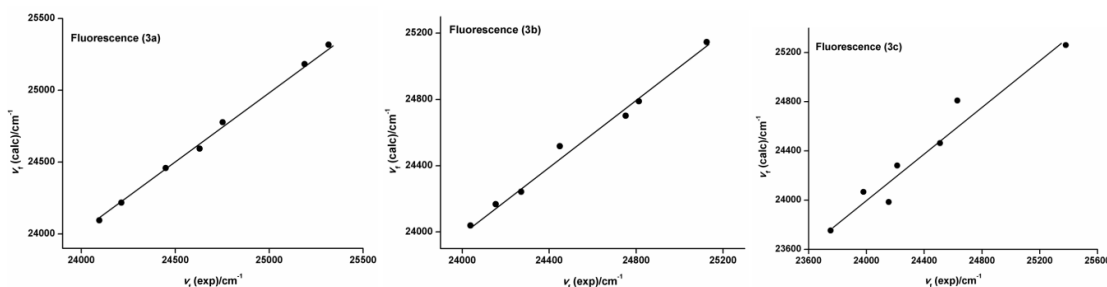


Fig. 10: Correlation between the experimental fluorescence values with the calculated values obtained by a multicomponent linear regression using the SA, SB, SP and SdP – scale (Catalán) solvent parameters for **3a**, **3b** and **3c**.

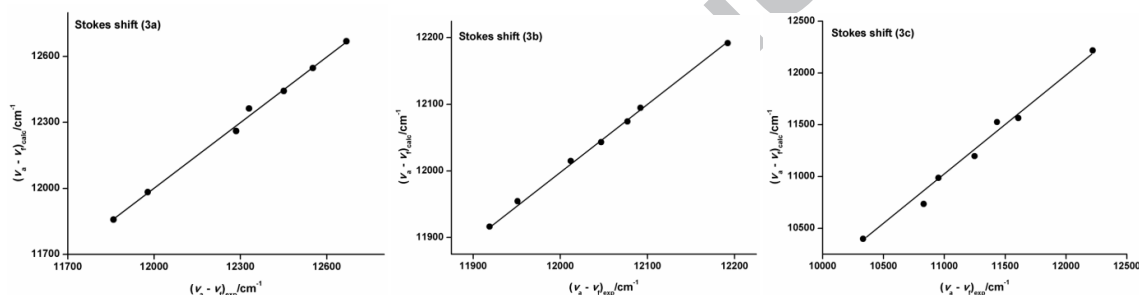


Fig. 11: Correlation between the experimental Stokes shift values with the calculated values obtained by a multicomponent linear regression using the SA, SB, SP and SdP – scale (Catalán) solvent parameters for **3a**, **3b** and **3c**.

Compound **3a** showed a satisfactory fit for the solvent dependence of absorption maxima ($r = 0.99$) as the absorption maxima depend mainly on the solvent polarizability (a_{SA}) out of four Catalán parameters indicating that the increased solvent polarizability stabilizes **3a** in their ground state. According to the eq. 16, the change of absorption maximum of **3b** depends on all the four solvent parameters with good correlation $r = 0.99$ but the solvent polarizability has the highest impact on the absorption maxima of **3b** indicating that the absorbance maxima shifted to lower energies with increasing polarizability of the solvents. Similarly, compound **3c** also showed a good correlation for the solvent dependence of the absorption maxima $r = 0.91$ in which absorption maxima depend on the solvent acidity (a_{SA}) indicating that there is hydrogen bonding between the C=O group of **3c** with the hydrogen of polar protic solvents. A good correlation of **3a**, **3b** and **3c** was observed $r = 0.99$, 0.99 and 0.95 , respectively for the solvent dependence of fluorescence maxima which depends on the two solvent parameters (c_{SP} , d_{SDP}) and negligibly on other two coefficients (a_{SA} , b_{SB}). However, the solvent

polarizability (ϵ_{SP}) has higher effect than solvent dipolarity (d_{SP}), suggesting that the emission maxima of all the three compounds is stabilized by increase in solvent polarizability (ϵ_{SP}).

The Stokes shift of compounds **3a**, **3b** and **3c** also showed an excellent fit with $r = 0.99$, 0.99 and 0.99 , respectively. The Stokes shift depends not only on the dipolarity but also on the solvent acidity. However, the impact of solvent acidity is lower than that of solvent dipolarity indicating that the Stokes shift increases with dipolarity.

3.3. Comparison of the calculated absorption spectra with experiment

On the basis of fully optimized ground-state structures (Fig. 2), TDDFT calculations using B3LYP-6-311G (d, p) basic set have been used to determine the HOMO-LUMO energy gap and also the electronic transitions for **3a**, **3b** and **3c**. The calculated results of oscillator strength (f), frequency, wavelength and energies of HOMO-LUMO orbitals are listed in Table 5.

Table 5: Selected vertical excitations calculated by the TDDFT (B3LYP) method for **3a**, **3b** and **3c**

Exp.	TD-DFT (B3LYP/6-311G (d,p))				Energies (a.u.)
	λ_{exc} (nm)	λ_{exc} (nm)	E_{exc} (eV)	F Character	
3a		287.65	4.3103	0.0006	H \rightarrow L+2 (57%), H \rightarrow L+5 (30%) $E_{HOMO} = -0.25795$
	270	278.66	4.4494	0.0029	H \rightarrow L (70%) $E_{LUMO} = -0.01863$
		264.98	4.6789	0.0001	H-6 \rightarrow L+1 (11%), H-5 \rightarrow L (64%), $\Delta E = -0.23932$ H-1 \rightarrow L (20%)
3b		287.53	4.3120	0.0006	H \rightarrow L+2 (56%), H \rightarrow L+5 (33%) $E_{HOMO} = -0.25663$
	272	273.37	4.5355	0.0035	H \rightarrow L (C=O) (70%) $E_{LUMO} = -0.01630$
		266.06	4.6600	0.0000	H-5 \rightarrow L (65%), H-4 \rightarrow L (16%), $\Delta E = -0.24033$ H-1 \rightarrow L (15%)
3c		386.73	3.2060	0.0000	H-1 \rightarrow L (69%) $E_{HOMO} = -0.23094$
	282	331.52	3.7398	0.0043	H \rightarrow L (69%), H-1 \rightarrow L (13%), $E_{LUMO} = -0.09586$ H-2 \rightarrow L (10%) $\Delta E = -0.13508$
		302.43	4.0996	0.0013	H-2 \rightarrow L (62%)

The TDDFT calculations in gas phase show a strong absorption band at 278 nm for **3a**, 273 nm for **3b** and 331 nm for **3c** which are in good agreement with the experimental absorption bands at 270 nm, 272 nm and 282 nm in chloroform, respectively. These absorption bands

indicate the existence of HOMO to LUMO transition. On the basis of the calculated molecular orbital coefficients, H→L electronic transition has been assigned as $\pi\rightarrow\pi^*$ for **3a**, **3b** and $n\rightarrow\pi^*$ for **3c** because of the presence of lone pair on sulphur in **3c**.

Fig. 12 shows 3D surface plots of the highest occupied molecular orbitals (HOMO), the lowest unoccupied molecular orbitals (LUMO) for compounds **3a**, **3b** and **3c**. In case of **3a** and **3b**, it can be seen that the HOMOs are mainly localized on the phenyl ring, whereas the LUMOs are localized over the barbituric acid moiety, suggesting a strong propensity for intramolecular charge transfer from the electron-donor phenyl ring to the electron acceptor C=O of amidic linkage, and therefore correspond to $\pi\rightarrow\pi^*$ transitions. In case of **3c**, HOMOs are mainly localized over the lone pair on sulphur atom and LUMOs are localized over the thiobarbituric acid moiety, indicating the occurrence of intramolecular charge transfer from lone pair of sulphur atom to the C=O of thiobarbituric acid, confirming the $n\rightarrow\pi^*$ transition.

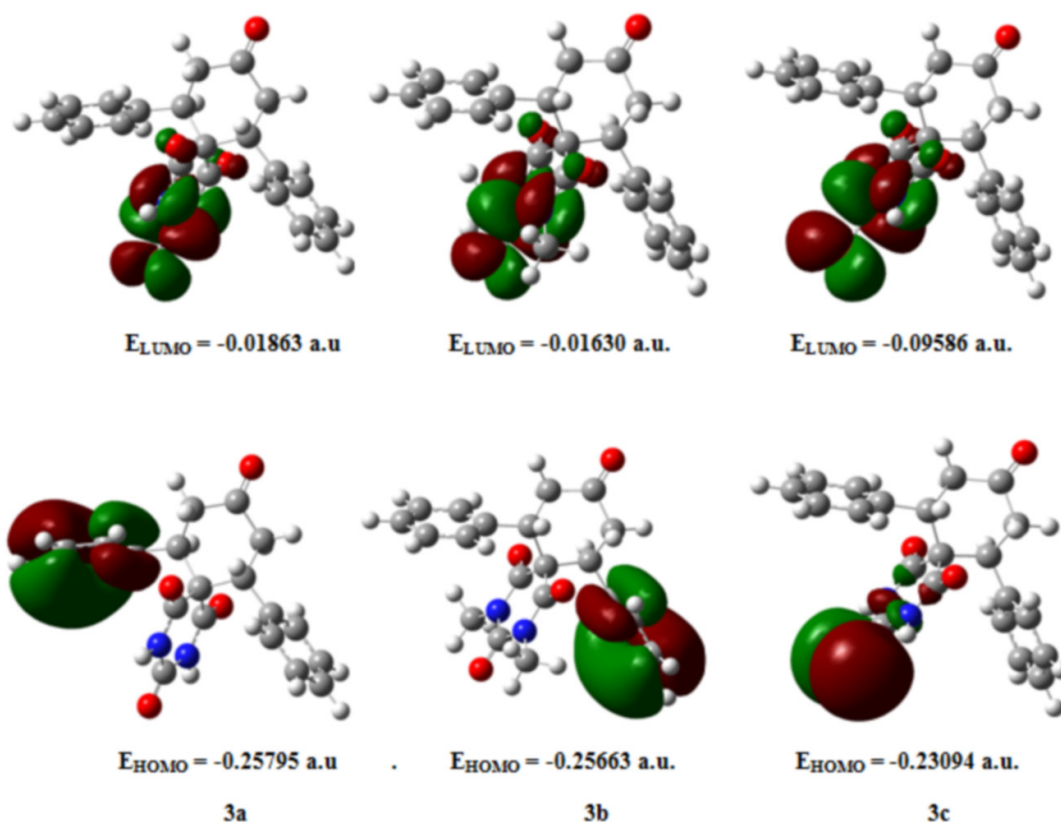


Fig. 12: The distribution of the HOMO and the LUMO over the molecules of **3a**, **3b** and **3c** calculated with TDDFT (B3LYP/6-311G (d,p)).

4. Conclusion

In conclusion, a new protocol for the synthesis of diazapiro compounds has been developed using TBAB in water:ethanol under reflux. Photophysical properties of three diazapiro compounds have been studied in the solvents of different polarity and the results showed that these fluorophores exhibit large Stokes shifts in polar protic solvent methanol. It has been found that the absorption and the fluorescence spectra of the compounds shift to lower energy as solvent polarity increases, confirming a $\pi \rightarrow \pi^*$ transition. Lippert–Mataga plot and the Reichardt’s plot of these compounds in solvents of different polarity illustrated linearity with good correlation. We found that all the three molecules possess higher dipole moment values in the excited state than the ground state. Moreover, the new four-parameter Catalán solvent scale which takes into account acidity, basicity, polarizability and dipolarity of the solvent, was also applied. The solvent parameter, namely solvent polarizability (c_{sp}) contributes majorly in stabilizing diazapiro compounds in the excited state. The frontier molecular orbitals have been visualized and the HOMO–LUMO energy gap has been calculated. The calculated HOMO and LUMO energies show that charge transfer occur within the molecule.

Acknowledgments

KA thanks CSIR, New Delhi, India for the grant of Junior and Senior Research Fellowships. The authors also thank Gaussian for providing us Gaussian 09 software.

References

- [1] M.F. Broglia, S.G. Bretolotti, C.M. Previtali, H.A. Montejano, *J. Photochem. Photobiol. A* 180 (2006) 143-149.
- [2] V.E. Nicotra, M.F. Mora, R.A. Iglesias, A.M. Baruzzi, *Dyes and Pigments* 76 (2008) 315-318.
- [3] N.R. Patil, R.M. Melavanki, S.B. Kapatkar, N.H. Ayachit, J. Saravanan, *J. Fluoresc.* 21 (2011) 1213-1222.
- [4] A.A. El-Rayyes, T. Htun, *Spectrochim. Acta Part A* 60 (2004) 1985-1989.
- [5] (a) K. Aggarwal, J.M. Khurana, *J. Photochem. Photobiol., A* 276 (2013) 71-82. (b) K. Guzow, A. Ceszak, M. Kozarzewska, W. Wiczak, *Photochem. Photobiol. Sci.* 10 (2011) 1610-1621.
- [6] A. Mallick, S. Maiti, B. Haldar, P. Purkayastha, N. Chattopadhyay, *Chem. Phys. Lett.* 371 (2003) 688-693.
- [7] M.K. Saroj, N. Sharma, R.C. Rastogi, *J. Mol. Struct.* 1012 (2012) 73-86.

- [8] R. M. Melavanki, N.R. Patil, S.B. Kapatkar, N.H. Ayachit, S. Umapathy, J. Thipperudrappa, A.R. Nataraju, *J. Mol. Liq.* 158 (2011) 105-110
- [9] M.S. Zakerhamidi, S.A. di-Kandjani, M. Moghadam, E. Ortyl, S. Kucharski, *Spectrochim. Acta Part A* 85 (2012) 105-110.
- [10] Y.T. Varma, S. Joshi, D.D. Pant, *J. Mol. Liq.* 179 (2013) 7-11.
- [11] J. Jayabharathi, V. Kalaiarasi, V. Thanikachalam, K. Jayamoorthy, *J. Fluoresc.* 24 (2014) 599-612.
- [12] J.S. Kadadevarmath, G.H. Malimath, N.R. Patil, H.S. Geethanjali, R.M. Melavank, *Can. J. Phys.* 91 (2013) 1107-1113.
- [13] (a) S.D. Choudhury, S. Basu, *Chem. Phys. Lett.* 371 (2003) 136-140; (b) R. Kakkar, V. Katoch, *J. Mol. Struct. (Theochem)* 578 (2002) 169-175.
- [14] A. Grofsik, M. Kubinyi, A. Ruzsinszky, T. Veszpremi, W.J. Jones, *J. Mol. Struct.* 555 (2000) 15-19.
- [15] E. Lippert, *Z. Naturforsch.* 10 (1955) 541-545.
- [16] N.G. Bakshiev, *Opt. Spektrosk.* 16 (1964) 821-832.
- [17] A. Kawski, *Z. Naturforsch.* 57a (2002) 255-262.
- [18] A. Chamma, P. Viallet, *C.R. Acad. Sci. Paris Ser. C* 270 (1970)1901-1910.
- [19] J. Czekalla, *Chimia* 15 (1961) 26-31.
- [20] J. Czekalla, *Zeitschrift fuer Elektrochemie und Angewandte Physikalische Chemie* 64 (1960) 1221-1228.
- [21] J.R. Lombardi, *J. Am. Chem. Soc.* 92 (1970) 1831-1833.
- [22] M.P. De Haas, J.M. Warman, *Chem. Phys.* 73 (1982) 35-53.
- [23] A. Kawski, B. Kukliński, P. Bojarski, *Z. Naturforsch.* 55a (2000) 550-554.
- [24] R Pradhan, M. Patra, A. K. Behera, B. K. Mishra, R. K. Behera, *Tetrahedron* 62 (2006) 779-828.
- [25] (a) S. Sivakumar, R.R. Kumar, M.A. Ali, T.S. Choon, *Eur. J. Med. Chem.* 65 (2013) 240-248; (b) G. Bhaskar, Y. Arun, C. Balachandran, C. Saikumar, P.T. Perumal, *Eur. J. Med. Chem.* 51 (2012) 79-91.
- [26] L.L. Brunton, J.S. Lazo, K.L. Parker, I. Buxton, D. Blumenthal (2006) Goodman and Gilman's The pharmacological basis of therapeutics. 11th eds, The McGraw- Hill Companies Inc.
- [27] M.W. Johns, *Drugs* 9 (1975) 448-478.
- [28] C. Uhlmann, W. Froscher, *CNS Neurosci. Ther.* 15 (2009) 24-31.

- [29] (a) D. Theford, A.P. Chorton, J. Hardman, *Dyes Pigments* 59 (2003) 185-191. (b) S. Wang, S.-H. Kim, *Dyes Pigments* 80 (2009) 314-320.
- [30] D. Popov, B. Thorell, *Stain Technol.* 53 (1978) 246-247.
- [31] D. Popov, B. Thorell, *Stain Technol.* 57 (1982) 143-150.
- [32] R. K. Behera, A. K. Behera, R. Pradhan, A. Pati, M. Patra, *Synth. Commun.* 36 (2006) 3729-3742.
- [33] R. K. Behera, A. K. Behera, R. Pradhan, A. Pati, M. Patra, *Phosphorus, Sulfur Silicon Relat. Elem.* 184 (2009) 753-765.
- [34] S. Kesharwani, N.K. Sahu, D.V. Kohli, *Pharm. Chem. J.* 43 (2009) 315-319.
- [35] B. Goel, S. Sharma, K. Bajaj, D. Bansal, T. Singh, N. Malik, S. Lata, C. Tyagi, H. Panwar, A. Agarwal, A. Kumar, *Indian J Pharm Sci.* 67 (2005) 194-199.
- [36] A.N. Osman, M.M. Kandeel, M.M. Said, E.M. Ahmed, *Indian J. Chem. Sect B.* 35B (1996) 1073-1078.
- [37] (a) D.B. Ramachary, M. Kishor, G.B. Reddy, *Org. Biomol. Chem.* 4 (2006) 1641-1646; (b) J.M. Khurana, R. Arora, S. Satija, *Heterocycles* 71 (2007) 2709-2716.
- [38] A.D. Becke, *J Chem Phys* 98 (1993) 5648-5650.
- [39] M.J. Frisch, G.W. Trucks, H.B. Schlegel, *et al.* (2009) GAUSSIAN 09, Revision A.02, Gaussian Inc., Wallingford, CT.
- [40] S. Miertuš, E. Scrocco, J. Tomasi, *Chem. Phys.* 55 (1981) 117-129.
- [41] S. Miertuš, J. Tomasi, *Chem. Phys.* 65 (1982) 239-245.
- [42] J. Tomasi, B. Mennucci, R. Cammi, *Chem. Rev.* 105 (2005) 299-3000.
- [43] E. Lippert, *Z Elektrochem* 61 (1957) 962-975.
- [44] N. Mataga, Y. Kaifu, M. Koizumi, *Bull. Chem. Soc.* 29 (1956) 465-470.
- [45] C. Reichardt, T. Welton, *Solvents and Solvent Effects in Organic Chemistry* (2011) Wiley VCH, Weinheim.
- [46] M. Ravi, T. Soujanya, A. Samanta, T.P. Radhakrishnan, *J. Chem. Soc., Faraday Trans.* 91 (1995) 2739-2742.
- [47] S. Jana, S. Dalapati, S. Ghosh, S. Kar, N. Guchhait, *J. Mol. Struct.* 998 (2011) 136-143.
- [48] M.J. Kamlet, J.L.M. Abboud, M.H. Abraham, R.W. Taft, *J. Org. Chem.* 48 (1983) 2877-2880.
- [49] J. Catalán, *J. Phys. Chem. B* 113 (2009) 5951-5960.

Figures Caption

Fig. 1: Structures of compounds **3a**, **3b** and **3c**.

Fig. 2: Optimized geometries for the lowest-lying state (S_0) of **3a**, **3b** and **3c** at the B3LYP/6-311G (d,p) level.

Fig. 3: Absorption and fluorescence spectra of compound **3a** in MeOH, ACN, DMF, DCM, CHCl_3 , DIOX and *n*-HEPT. Excitation wavelength: 270 nm.

Fig. 4: Absorption and fluorescence spectra of compound **3b** in MeOH, ACN, DMF, DCM, CHCl_3 , DIOX and *n*-HEPT. Excitation wavelength: 272 nm.

Fig. 5: Absorption and fluorescence spectra of compound **3c** in MeOH, ACN, DMF, DCM, CHCl_3 , DIOX and *n*-HEPT. Excitation wavelength: 280 nm.

Fig. 6 (a) Plot of Stokes shift vs. Orientation polarizability (Δf) of **3a**, **3b** and **3c**. (b) Plot of Stokes shift vs. Reichardt's solvent polarity function E_T^N of **3a**, **3b** and **3c**.

Fig. 7: (a) Variation of Stokes shift with F_1 (ϵ , n) by using Bakhshiev's equation in different solvents for **3a**, **3b** and **3c**. (b) The variation of arithmetic mean of $\bar{\nu}_a$ and $\bar{\nu}_f$ with F_2 (ϵ , n) by using Kawski-Chamma-Viallet's equation in different solvents for **3a**, **3b** and **3c**.

Fig. 8: Possible resonating or tautomeric structures of **3a**, **3b** and **3c**.

Fig. 9: Correlation between the experimental absorption values with the calculated values obtained by a multicomponent linear regression using the SA, SB, SP and SdP – scale (Catalán) solvent parameters for **3a**, **3b** and **3c**.

Fig. 10: Correlation between the experimental fluorescence values with the calculated values obtained by a multicomponent linear regression using the SA, SB, SP and SdP – scale (Catalán) solvent parameters for **3a**, **3b** and **3c**.

Fig. 11: Correlation between the experimental Stokes shift values with the calculated values obtained by a multicomponent linear regression using the SA, SB, SP and SdP – scale (Catalán) solvent parameters for **3a**, **3b** and **3c**.

Fig. 12: The distribution of the HOMO and the LUMO over the molecules of **3a**, **3b** and **3c** calculated with TDDFT (B3LYP/6-311G (d,p)).

Graphical Abstract

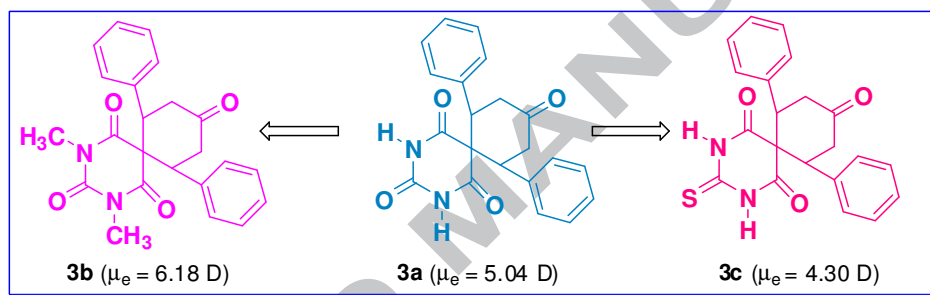
Synthesis, photophysical studies, solvatochromic analysis and TDDFT calculations of Diazaspiro compounds

Komal Aggarwal and Jitender M. Khurana*

Department of Chemistry, University of Delhi, Delhi-110007, India

*Corresponding author. Tel.: +91 11 2766772; fax: +91 1 27667624

E-mail addresses: jmkhurana1@yahoo.co.in; jmkhurana@chemistry.du.ac.in



HIGHLIGHTS

- Diazaspiro compounds have been synthesized *via* double Michael addition.
- The solvent effect has been investigated by using the Lippert–Mataga, Reichardt methods and Catalán polarity scales.
- μ_g and μ_e have been calculated by solvatochromic method.
- The HOMO and LUMO energies have been calculated.

ACCEPTED MANUSCRIPT